JOINT EUROPEAN TORUS JET

JET–P(90)02

D.F.H. Start, D.V. Bartlett, V.P. Bhatnagar, D.J. Campbell, C.D. Challis,
A.D. Cheetham, S. Corti, A.W. Edwards, L-G. Eriksson, R.D. Gill,
N. Gottardi, T. Hellsten, J. Jacquinot, J.O'Rourke, M.J. Mayberry,
D. Moreau, F.G. Rirnini, N.A. Salmon, P. Smeulders,
M. von Hellermann and JET Team

Electron Absorption of Fast Magnetosonic Waves by Transit Time Magnetic Pumping in the JET Tokamak

Electron Absorption of Fast Magnetosonic Waves by Transit Time Magnetic Pumping in the JET Tokamak

D.F.H. Start, D.V. Bartlett, V.P. Bhatnagar, D.J. Campbell, C.D. Challis, A.D. Cheetham, S. Corti, A.W. Edwards, L-G. Eriksson, R.D. Gill, N. Gottardi, T. Hellsten[1], J. Jacquinot, J.O'Rourke, M.J. Mayberry[2], D. Moreau[3], F.G. Rirnini, N.A. Salmon, P. Smeulders, M. von Hellermann and JET Team*

JET-Joint Undertaking, Culham Science Centre, OX14 3DB, Abingdon, UK

[1]Royal Institute of Technology, S-10044, Stockholm, Sweden
[2]General Atomics, San Diego, California, U.S.A.
[3]CEA Centre d'Etudes Nucleaires de Cadarache, France
** See Appendix 1*

Preprint of Paper to be submitted for publication in Nuclear Fusion

Preprint of a paper to be submitted to Nuclear Fusion Letters

ELECTRON ABSORPTION OF FAST MAGNETOSONIC WAVES BY TRANSIT TIME MAGNETIC PUMPING IN THE JET TOKAMAK

D F H Start, D V Bartlett, V P Bhatnagar, D J Campbell, C D Challis, A D Cheetham, S Corti, A W Edwards, L-G Eriksson, R D Gill, N Gottardi, T Hellsten[1], J Jacquinot, J O'Rourke, M J Mayberry[2], D Moreau[3], F G Rimini, N A Salmon, P Smeulders and M von Hellermann

JET Joint Undertaking, Abingdon, Oxon, OX14 3EA, UK

[1]Royal Institute of Technology S-10044, Stockholm, Sweden
[2]General Atomics San Diego, California, USA
[3]CEA Centre d'Etudes Nucléaires de Cadarache, France

ABSTRACT Direct electron damping of low frequency fast magnetosonic waves has been observed in the centre of high beta hydrogenic JET plasmas where transit time magnetic pumping is a significant component in the electron-wave interaction mechanism. The electron heating power profile was peaked on axis, extended across almost half the minor radius and accounted for 22±5% of the total radiofrequency power coupled to the plasma. Outside this region the fast wave was absorbed by hydrogen ions at the second harmonic cyclotron resonance which was situated 0.4m inboard of the magnetic axis.

Tokamak fusion reactors will almost certainly require some form of non-inductive current drive, either for complete steady state operation or for current profile control to maintain plasma stability. Direct electron damping of low frequency (~ 20 MHz) fast magnetosonic waves could provide the most effective method of driving such currents. Theoretical work by Fisch and Karney [1] first showed that such a scheme has an even greater efficiency than lower hybrid current drive which, so far, has achieved 2 MA of plasma current in the JT-60 Tokamak [2]. The efficiency enhancement depends on the parallel energy of the resonant electrons and is 70 % for thermal electrons reducing to 15 % at ten times the thermal energy. Furthermore, the fast wave can propagate to the centre of high temperature, high density reactor plasmas, a region forbidden to lower hybrid waves according to the

Stix-Golant accessibility criterion [3, 4]. The disadvantage of the fast wave method in present size experiments, and the reason for its slow experimental development, is the weak electron damping relative to other possible absorption mechanisms, notably ion cyclotron damping.

The interaction between the fast wave and electrons is a coherent combination of transit time magnetic pumping (TTMP) and electron Landau damping (ELD) [5]. Both components accelerate electrons along the magnetic field lines and absorption takes place at the Landau resonance for which $\omega = k_{\|} v_{\|}$. The quantities $k_{\|}$ and $v_{\|}$ respectively, are the components of the wave vector and electron velocity parallel to the magnetic field and ω is the angular frequency. Recently, detailed theoretical treatments of the absorption have been given by Moreau et al. [6] and by Chiu et al. [7] for frequencies ranging from below the ion cyclotron frequency up to the lower hybrid frequency. These authors find that the parameter $\alpha = T_e\omega_{pi}^2/m_e c^2\omega^2$ plays a key role in determining the relative strength of the TTMP and ELD interactions. In the above equation, T_e is the electron temperature, ω_{pi} is the ion plasma frequency and $m_e c^2$ is the electron rest energy. For example, the force $F_{\|}$, acting on an electron with $v_{\|} > v_e$ is given by

$$F_{\|}(E_{\perp}) = ie\phi k_{\|}\omega^2(\omega_{ce}\omega_{ci})^{-1}.[1 + \alpha - \alpha E_{\perp}/\langle E_{\perp}\rangle] \qquad (1)$$

where v_e is the electron thermal velocity, $E_{\perp}$ is the electron energy perpendicular to the magnetic field, ϕ is the RF electric potential, ω_{ce} is the electron cyclotron frequency, ω_{ci} is the ion cyclotron frequency and $\langle E_{\perp}\rangle$ is the perpendicular energy averaged over the electron distribution function. The terms $1 + \alpha$ and $\alpha E_{\perp}/\langle E_{\perp}\rangle$ are due to ELD and TTMP respectively. Thus, for an electron whose magnetic moment (μ) is thermal, α is the ratio of the $\mu\Delta B$ force to the total force produced by the combined ELD and TTMP components acting in opposite directions. For $\alpha >> 1$ (low frequency waves and high beta plasma), the interaction takes place principally by TTMP in the case of electrons with $E_{\perp}$ greater than $\langle E_{\perp}\rangle$. Conversely, ELD is the stronger component for electrons with $E_{\perp}$ less than $\langle E_{\perp}\rangle$. Also in the limit $\alpha >> 1$ the current drive efficiency has the enhanced value found by Fisch and Karney and the damping [6,7] is given by

$$\frac{2k_{\perp i}}{|k_{\perp}|} = \frac{\sqrt{\pi}}{2}\beta_e\xi e^{-\xi^2} \qquad (2)$$

where $k_{\perp}$ is the wavevector perpendicular to the magnetic field, $k_{\perp i}$ is the imaginary part of $k_{\perp}$, β_e is the electron beta and $\xi (= \omega/k_{\|}v_e)$ is the phase

velocity normalised to the electron thermal velocity. As can be seen from equation 2, the strongest absorption occurs at maximum β_e and at a phase velocity of $v_e/\sqrt{2}$.

In the regime $\alpha<<1$ (high frequency waves and low beta plasma), ELD dominates the interaction for all values of $E_\parallel$, and the current drive efficiency is the same as for lower hybrid waves. This regime contains all the fast wave current drive experiments carried out so far [6], on ACT-1 [8], JIPP T-IIU [9, 10], JFT-2M [11] and PLT [12]. In all cases the value of α was less than 0.1 and for each experiment the frequency was at least an order of magnitude greater than the ion cyclotron frequency. In reactor plasmas such high frequency schemes could suffer from harmonic cyclotron damping by alpha particles. A more attractive alternative [13, 14] would be to use a frequency just below the lowest cyclotron frequency, ω_{cT} in a D-T reactor, thereby avoiding all cyclotron damping and benefiting from the improved current drive efficiency. Such a scenario is typically characterised by α ~ 50. Clearly there is a need to establish an experimental basis for these high beta schemes at the low frequency end of the ion cyclotron spectrum. JET parameters provide an opportunity for such experiments and evidence for combined TTMP + ELD absorption has been found in the centre of ^{4}He discharges with on-axis ^{3}He minority ICRH [15]. The present letter describes experiments in JET hydrogen plasmas where the hydrogen second harmonic cyclotron resonance was placed well inboard of the magnetic axis so that no cyclotron resonance or mode conversion layer existed inside a minor radius of 0.4m. Direct electron damping has been observed in this central region and is in good agreement with the theoretically predicted absorption of the fast wave by TTMP+ELD. Furthermore, these discharges gave a value of α = 3 so that TTMP was a significant component in the acceleration of the resonant electrons.

The experiments were carried out in JET double null X-point discharges with a plasma current of 2 MA. A poloidal cross section of this type of discharge is shown in Fig. 1. The last closed flux surface closely follows the RF antenna curvature allowing optimal coupling to the fast wave. The hydrogen target plasma was heated simultaneously by both RF and neutral beam injection (NBI) for a period of 2 sec. The NBI heating consisted of 4 MW of 80 keV deuterium atoms. The RF power was launched using the ion cyclotron resonant heating (ICRH) antennae and was square wave modulated at 8 Hz between 3 MW and 9 MW. The frequency was 48 MHz and each antenna operated with dipole phasing. In

this mode, the launched power spectrum in $k_{\|}$ has a maximum at $k_{\|} = 7m^{-1}$ with a full width at half maximum, $\Delta k_{\|} = 7m^{-1}$.

For a central toroidal magnetic field (B_T) in vacuum of 1.34T the hydrogen second harmonic ion cyclotron resonance in the plasma is calculated to be at a major radius of 2.68m when paramagnetic and diamagnetic effects are taken into account. The position of this resonance layer is shown in Fig. 1. The flux surface ψ_c which just touches the resonance encloses a substantial central plasma volume that is free from ion cyclotron and mode conversion layers. In this situation central damping of the fast wave can only occur through the TTMP/ELD process. Studies of the direct electron heating in this region were carried out using a multi-channel heterodyne electron cyclotron emission (ECE) radiometer [16] to observe the response of the electron temperature to the RF power modulation. This instrument views the plasma horizontally along the mid-plane and was tuned to detect second harmonic E-mode radiation. The spatial resolution due to the receiver spot size is about 0.08m. At $B_T = 1.34T$ the range of operation covers the plasma core region between major radii of 3.07m and 3.32m. In order to increase this range, data were also taken at $B_T = 1.44T$ for which the $\omega = 2\omega_{cH}$ resonance occurs at 2.87m and the ECE diagnostic scans from R = 3.30m to R = 3.58m. In this case the resonance intersects the flux surfaces covered by the ECE radiometer so that mode conversion at the second harmonic, as well as TTMP + ELD, can contribute to the prompt electron heating signal. However, with dipole antenna phasing the mode conversion component is small and, according to full wave calculations, accounts for only 1% of the total power absorption.

Typical plasma parameters obtained during the combined heating are shown in fig. 2. The electron density (n_e) and the temperature profiles were measured with the LIDAR Thomson scattering system [17]. Ion temperatures (T_i) were deduced from the Doppler broadening of charge exchange recombination radiation emitted by carbon impurity ions [18]. Both the T_e and T_i profiles are strongly peaked with on-axis values of 3.9 keV and 2.9 keV respectively. The density profile is much broader and has a central value of $2.2 \times 10^{19} m^{-3}$. The volume averaged, total beta for this discharge is 1.4% which is approximately 30% of the Troyon limit for kink modes [19].

An estimate of the single pass power absorption in the central plasma enclosed by ψ_c can be made using eqn. (2) and the parameters in fig. 2. The average electron temperature inside ψ_c is 2.8 keV giving an electron beta of

1.5%. A launched $k_{\parallel}$ of $7m^{-1}$ becomes $9m^{-1}$ in the plasma centre (since $k_{\parallel}R$ ~ constant) so that $\xi = 1.1$. Taking $k_{\perp} = \omega/v_A$, where v_A is the Alfvên speed, we obtain $2k_{\perp i} = 0.22m^{-1}$ which suggests that about 17% of the incident power will be absorbed on the first pass by TTMP/ELD inside a minor radius of 0.4m.

The response of T_e on axis to the RF power modulation can be seen in fig. 3 which shows the ECE radiometer signal together with the RF power trace. The presence of direct electron damping of the wave is revealed by a change in the slope ($\dot{T}_e$) of the sawtooth ramp at the time of the RF power is switched up or switched down. The step in the power per unit volume absorbed by the electrons is related to the discontinuity ($\Delta\dot{T}_e$) in the temperature slope through the expression $\Delta P_e = \frac{3}{2} n_e \Delta\dot{T}_e$, provided the heat transport remains continuous during the RF power transition and $\Delta\dot{n}_e = 0$. There is no detectable discontinuity in $\dot{n}_e$ and we can set an upper limit of $0.01MW/m^3$ on the error introduced by neglecting this component in the determination of the power density.

Values of ΔP_e obtained from $\Delta\dot{T}_e$ are plotted against major radius in fig. 4. The solid points show data for $B_T = 1.34T$ and the open points for $B_T = 1.44T$. The centrally peaked power deposition is as expected from the similar form of the β_e profile and the maximum power density is ~ $0.11\ MW/m^3$. When the data in fig. 4 is fitted with a gaussian shape, we find that the total modulated power absorbed within ψ_c is about 1.3 ± 0.3 MW. This corresponds to $22\pm5\%$ of the modulated input power which is somewhat larger than the above estimate based on eqn. (2).

Further profile information is obtained from soft X-ray measurements using imaging cameras which view the JET plasma from two orthogonal directions [20]. The data is tomographically inverted to produce emissivity profiles, $\varepsilon(R)$ in the mid-plane such as those shown in fig. 5. The change in slope $\Delta\dot{\varepsilon}$ is clearly seen in the plasma centre as the RF power is switched down at 52.12s. A profile of $\Delta\dot{\varepsilon}$ averaged over several RF power transitions is shown in fig. 6 and confirms the centrally peaked power deposition profile deduced from the ECE measurements. The error bars represent rms deviations. The maximum value of $\Delta\dot{\varepsilon}$ appears to be slightly displaced (0.07m) from the magnetic axis although this is within the uncertainties of the tomographic and equilibrium calculations. The profile of $\Delta\dot{\varepsilon}$ also shows subsidiary peaks outside the sawtooth inversion radius which could be due to electron heating

by mode conversion in the vicinity of the $\omega = 2\omega_{cH}$ resonance. However, the asymmetry in $\Delta\dot{\varepsilon}$ between the high and low field sides is difficult to explain especially as the emisivity, ε, has a symmetric profile.

The total power deposited in the plasma can be calculated from the modulated components of W_{dia} and W_{mhd}, the plasma energy content measurements given by the diamagnetic loop and Shafranov shift, respectively [21]. These diagnostics have different sensitivities to the parallel and perpendicular energies such that the total energy content is given by

$$\tilde{W}_{tot} = 1/3 \left(\tilde{W}_{dia} + 2\tilde{W}_{mhd}\right) \qquad (3)$$

where the tilde denotes the modulated component. For the present experiments the global energy confinement time, (τ_E) is 0.18s so that $\omega_m \tau_E \sim 9$, where ω_m is the fundamental angular frequency of the modulation. In this case the square wave amplitude of the absorbed power can be obtained from $\tilde{P}_{tot} = 2\omega_m \tilde{W}_{tot}/\pi$. The waveforms of $\tilde{W}_{dia}$ and $\tilde{W}_{mhd}$ are shown in fig. 7 for the experiments with $B_T = 1.34T$. Both signals have a peak/peak variation of 0.14MJ which gives $\tilde{P}_{tot} = 4.4$ MW compared with 5.8 MW of modulated input. Thus 77±10% of the coupled power is deposited in the bulk plasma where the energy confinement time exceeds ω_m^{-1} by almost an order of magnitude. This result, in conjunction with the direct electron heating measurements, suggests that a) most of the power absorption takes place at the hydrogen second harmonic resonance and b) a small amount of power is deposited in the plasma periphery where the sensitivity of the method is reduced by the poor energy confinement in the edge region.

The power density profile for direct electron damping is compared in fig. 8 with theoretical profiles based on ray tracing [22] and a self-consistent treatment of power deposition and velocity distribution using the PION code [23]. In addition to TTMP and ELD, both models take account of second harmonic cyclotron absorption. The PION code also includes mode conversion, although the latter is negligible in the present case with dipole antennae phasing. The theoretical direct electron heating profiles in fig. 8 correspond to a modulated input power of 4.4 MW which is the observed power deposited in the bulk plasma. The PION code predicts that 70±5% of the power is absorbed by the ions and 30±5% by direct electron damping. Inside ψ_c the predicted power absorbed by the electrons is 1.2±0.2 MW and this is in good agreement with the measured value of 1.3±0.3 MW. Also, the calculated self-consistent hydrogen ion distribution function has at least 90% of the

ions below the critical energy and this is consistent with the observed lack of velocity space anisotropy as shown by the equality of $\tilde{W}_{dia}$ and $\tilde{W}_{mhd}$: anisotropy begins to develop when the tail temperature exceeds the critical energy (~25keV in the present case) and ion-ion pitch-angle scattering is reduced. However, the predicted profile is much more peaked than the measured profile with a central power density of 0.3 MW/m^3 compared with the observed value of 0.11 MW/m^3. However it should be noted that the PION code assumes an idealized antenna current and does not take into account the gap in the central conductor on the equatorial plane which depletes the electric field near the axis. The ray tracing calculations predict that 38% of the input power is absorbed by electrons and 62% by ions. In this case, the second harmonic damping was obtained by using an average ion energy of 10keV as given by Fokker-Planck calculations. The electron heating profile is shown in fig. 8 and has a maximum slightly off-axis at a minor radius of 0.2m. This effect is due to the convergence of the rays towards a focus which is 0.2m on the high field side of the magnetic axis. The calculated power absorbed by the electrons inside ψ_c is 1.2MW in agreement with both the experiment and PION calculations.

In summary, we have observed collisionless electron damping of fast magnetosonic waves in the centre of JET hydrogen discharges when there is no competing mode conversion or ion cyclotron absorption within a minor radius of 0.4m. Outside this region, power was absorbed by the bulk ions at the $2\omega_{cH}$ resonance. The experimental conditions of high beta plasmas and a low frequency wave ensured that TTMP was a significant component in the wave electron interaction. The electron heating profile was determined from measurements of the ECE and soft X-ray response to RF power modulation. The maximum power density occurred on-axis but the profile was less peaked than that predicted by either ray tracing or the PION code calculations. The discrepancy is greatest in the latter case and could be due to the simplified antenna geometry assumed in the code. However, the total power absorbed by the electrons agrees well with theory.

ACKNOWLEDGEMENT

It is a pleasure to thank all our colleagues in the JET team for assistance in this work. Particular thanks go to the tokamak operating team and to the diagnostic groups involved in the measurements reported here.

REFERENCES

[1] Fisch N.J. and Karney C.F., Phys. Fluids 24 (1981) 27.

[2] Nagashima T. and the JT-60 team, Proceedings of the 7th Topical Conference on Applications of Radiofrequency Power to Plasmas, Kissimmee, USA 1978 p. 94.

[3] Stix T.H. The Theory of Plasma Waves, McGraw-Hill. New York, 1962.

[4] Golant V.E., Sov Phys. Tech Phys 16 (1972) 1980.

[5] Stix T.H., Nuclear Fusion 15 (1975) 737.

[6] Moreau D., O'Brien M.R., Cox M. and Start D.F.H., Proceedings of the 14th European Conference on Controlled Fusion and Plasma Physics, Madrid, Spain 1987 Vol. III p. 1007.

[7] Chiu S.C., Chan V.S., Harvey R.W. and Porkolab M., submitted to Nuclear Fusion.

[8] Goree J. et al, Phys Rev Lett 55 (1985) 1669.

[9] Ando R. et al, Nuclear Fusion 26 (1986) 1619.

[10] Ohkubo K. et al, Phys. Rev. Lett. 56 (1986) 2040.

[11] Yamamoto T. et al, Report JAERI-M 86-115 (1986).

[12] Pinsker R.I et al, in Applications of Radio Frequency Power to Plasmas (Proc 7th Top Conf., Kissimee, 1987), Bernabei S. and Motley R.W, eds., AIP (New York) 1987, p.175.

[13] Jacquinot J. et al, to be published.

[14] Hellsten T. and Moreau D., private communication.

[15] Eriksson L.G. and Hellsten T., Nuclear Fusion 29 (1989) 875.

[16] Salmon N.A., Bartlett D.V. and Costley A.E., Proceedings of the Joint Workshop on ECE and ECRH, Oxford UK 1987, Culham Laboratory report CLM ECR (1987).

[17] Salzmann H. et al, Nuclear Fusion Letters 27 (1987) 1925.

[18] Boileau A. et al, Plasma Physics and Controlled Fusion 31 (1989) 779.

[19] Smeulders P. et al, to be published.

[20] Edwards A.W. et al, Rev. Sci. Instr. 57(1986)2142.

[21] Christiansen J.P., Cordey J.G. and Muir D.G., Nuclear Fusion 29(1989)1505.

[22] Bhatnager V.P. et al, Nuclear Fusion 24 (1984) 955.

[23] Eriksson L.G. and Hellsten T., JET Report P(89)65.

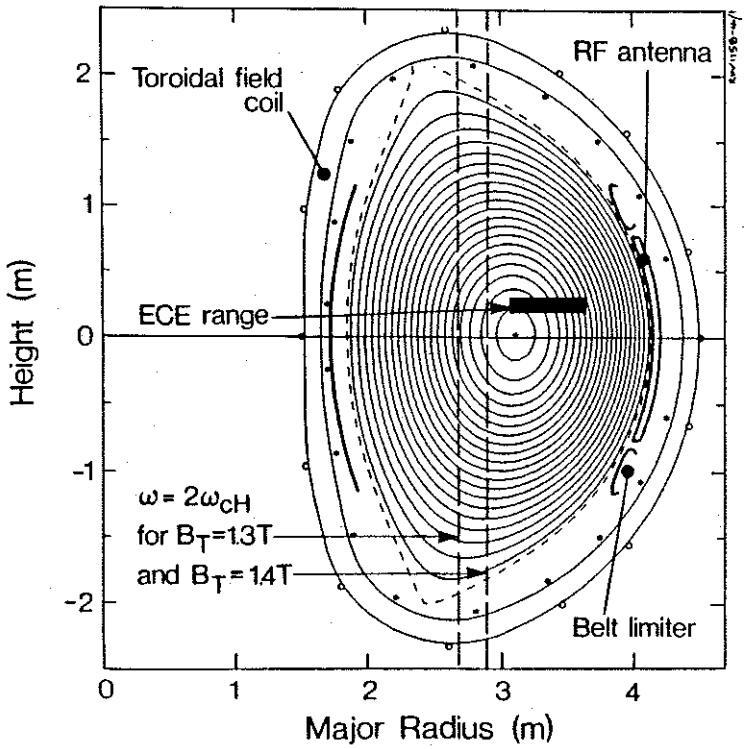

Fig. 1 Double-null X-point configuration in JET. The $\omega = 2\omega_{cH}$ resonance positions for $B_T = 1.34$ T and $B_T = 1.44$ T are shown together with corresponding operating ranges of the ECE diagnostic.

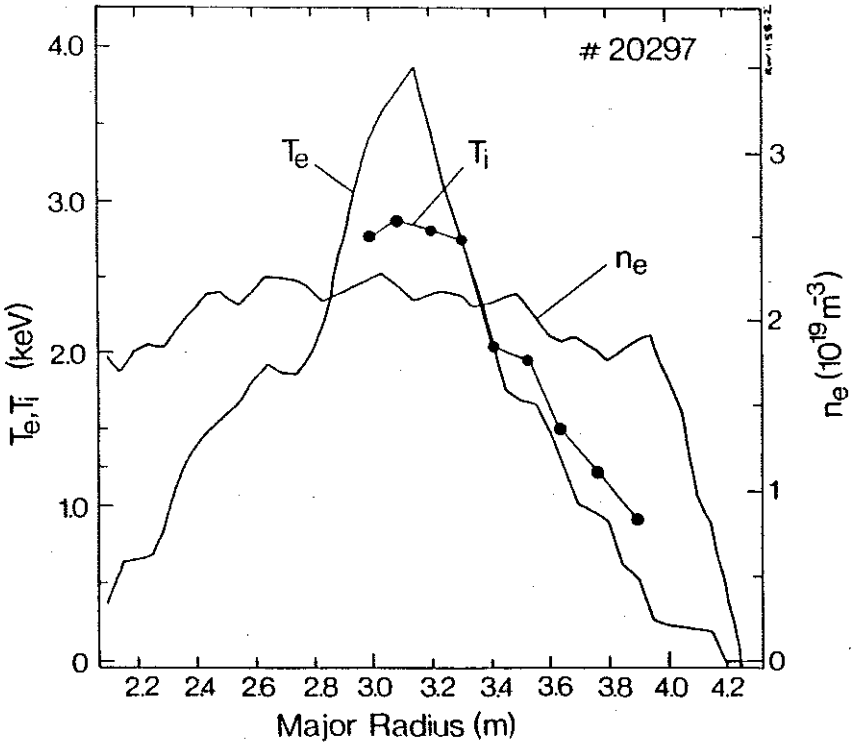

Fig. 2 Typical profiles of electron temperature (T_e), ion temperature (T_i) and electron density (n_e).

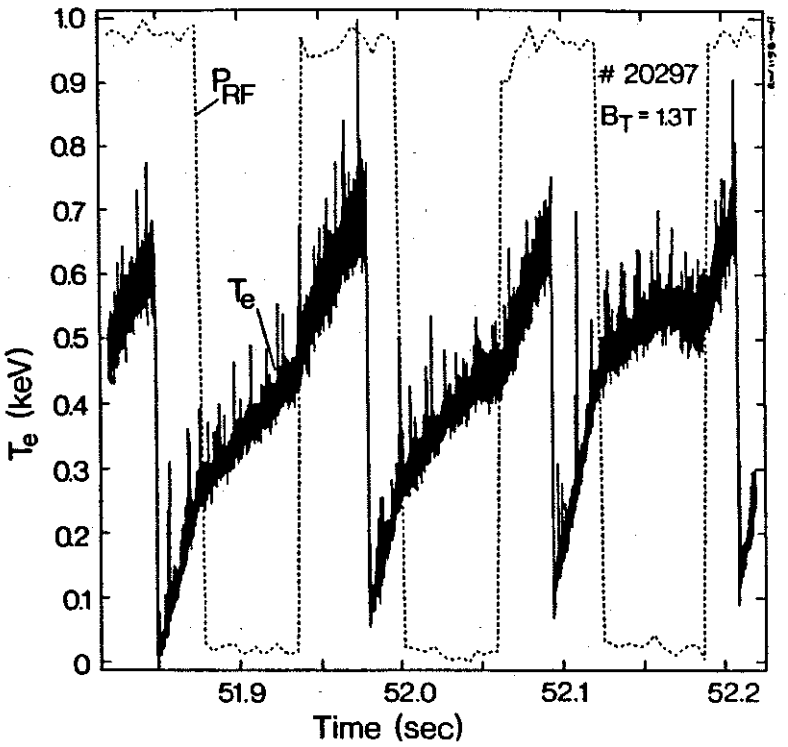

Fig. 3 Electron temperature response to modulated RF power as measured with the central ECE channel. Note the change in the time deriative of T_e at each RF power transition showing the presence of direct electron heating.

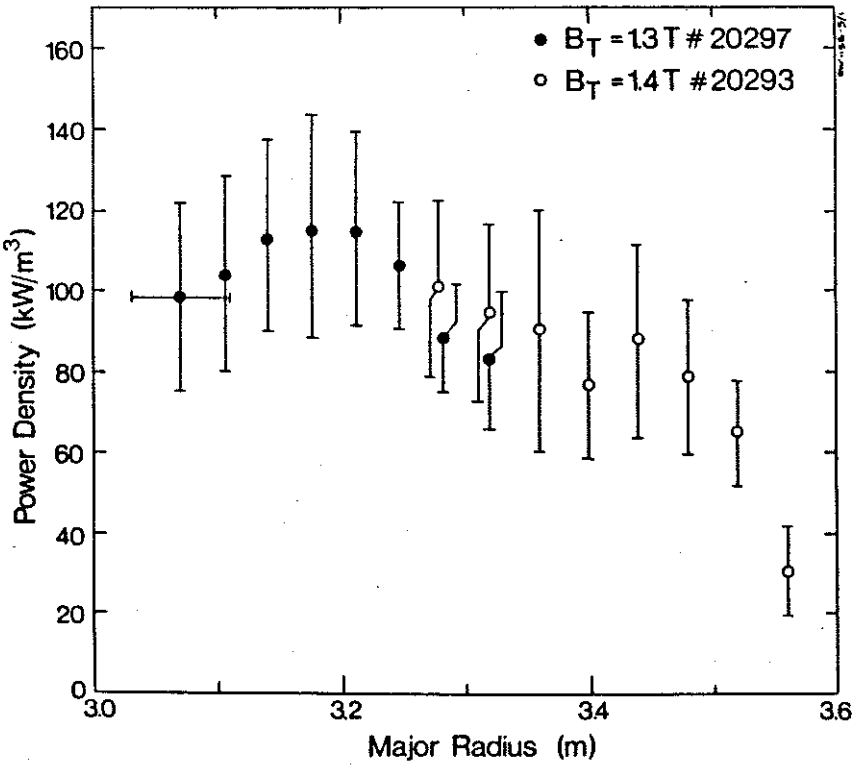

Fig. 4 Electron heating power density deduced from the ECE measurements and plotted against major radius for $B_T = 1.34$ T and $B_T = 1.44$ T. This profile corresponds to a height of 0.25 m above the median plane.

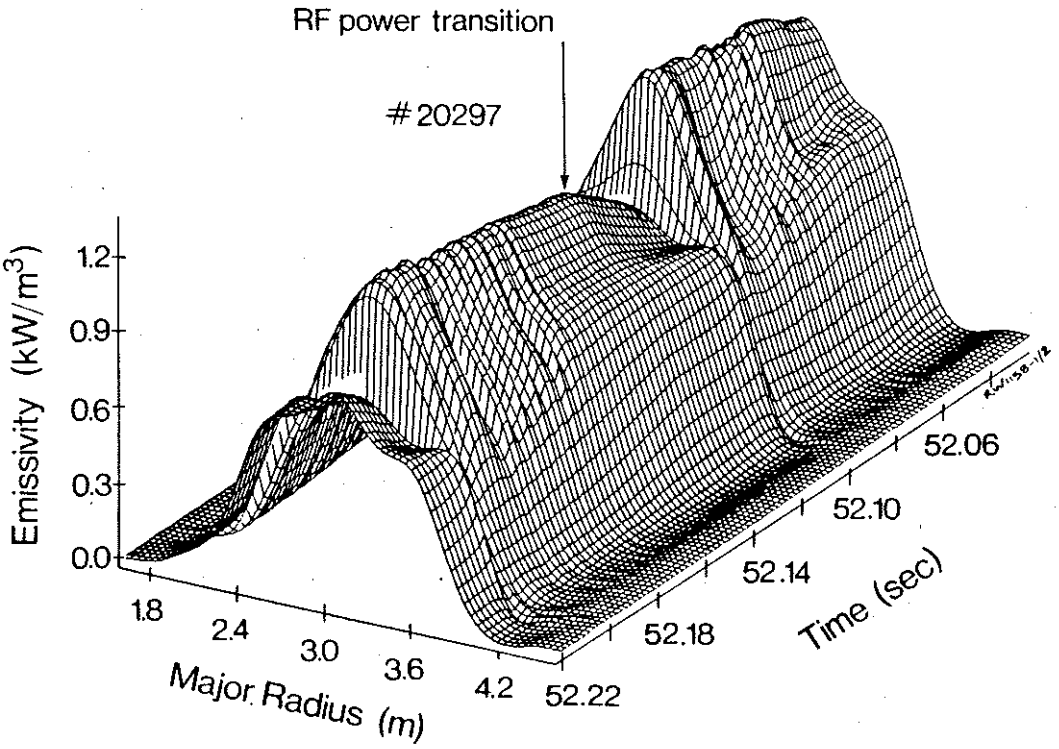

Fig. 5 Tomographically reconstructed soft X-ray emission profiles in the median plane. Sawtooth crashes occur at t=52.09 s and t=52.21 s and the RF power is switched down at t=52.12 s.

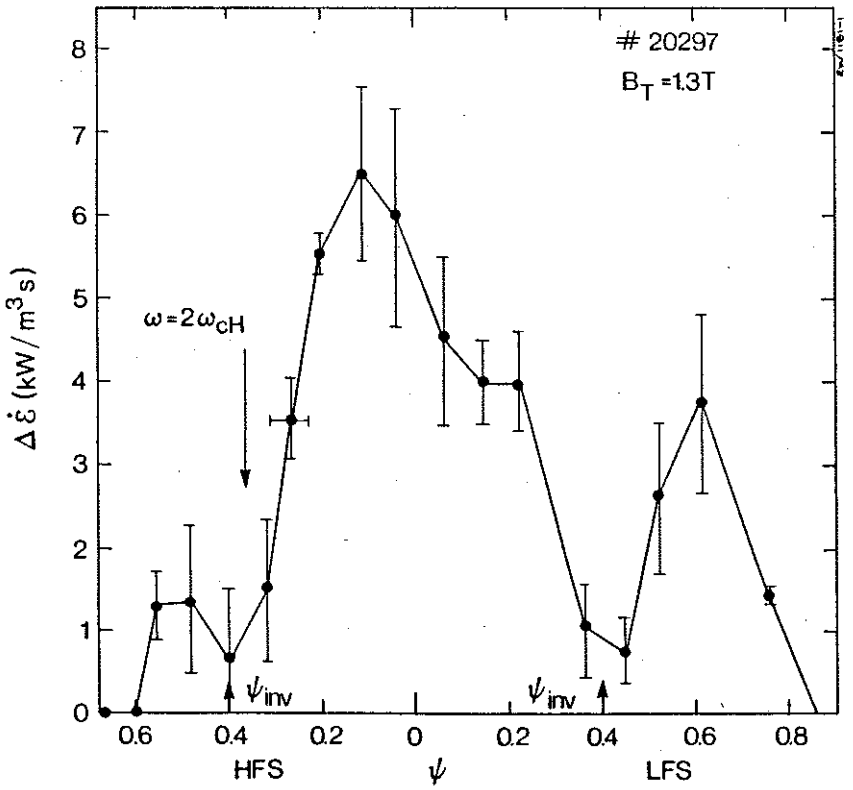

Fig. 6 Discontinuity in the time derivative of the soft X-ray emissivity which is caused by the RF power transition and which shows the electron heating to be peaked on-axis. The discontinuity was obtained from the median plane emissivity profiles shown in Fig. 5. The abscissa Ψ is the magnetic flux normalized to unity at the boundary. The labels HFS and LFS denote high field side and low field side respectively.

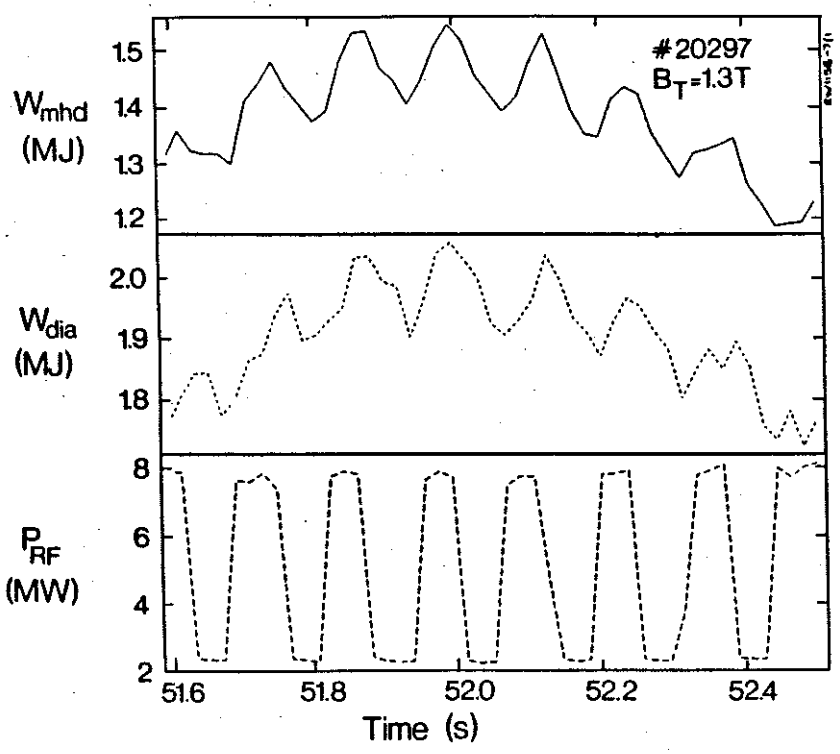

Fig. 7 Response of W_{dia} and W_{mhd} to RF power modulation.

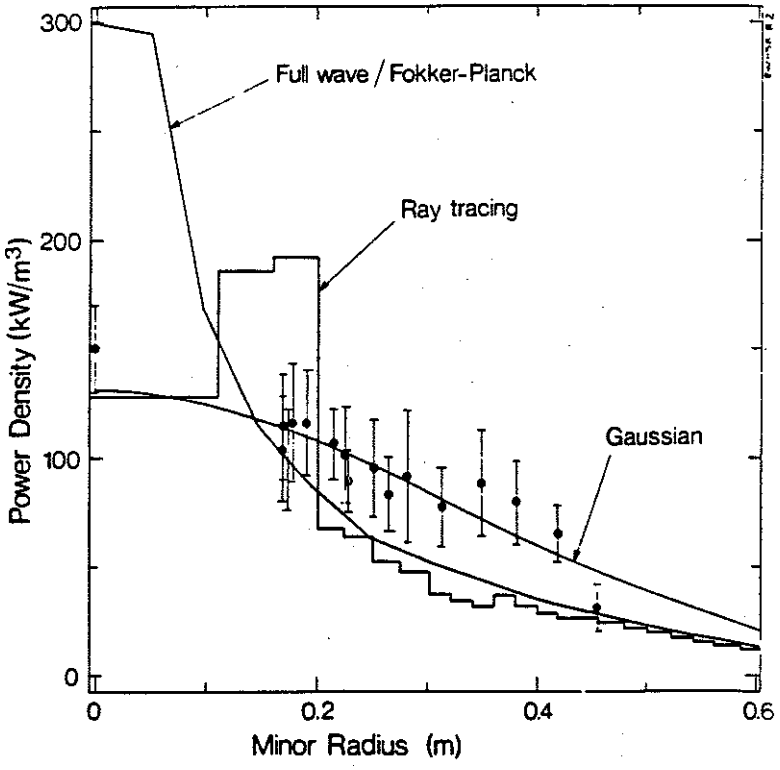

Fig. 8 Comparison of the observed direct electron heating power density profile in minor radius with theoretical profiles from ray tracing and PION code calculations. The central point was obtained from the soft X-ray data.